LETTER • OPEN ACCESS

Sea spray effects on typhoon prediction in the Yellow and East China Seas: case studies using a coupled atmosphere-ocean-wave model for Lingling (2019) and Maysak (2020)

View the article online for updates and enhancements.

You may also like

ENVIRONMENTAL RESEARCH
LETTERS

LETTER

Sea spray effects on typhoon prediction in the Yellow and East China Seas: case studies using a coupled atmosphere-ocean-wave model for Lingling (2019) and Maysak (2020)

Sinil Yang[1] , Hyo-Jun Bae[2], Mark Bourassa[3,4], Chaehyeon Chelsea Nam[3], Steven Cocke[4], DW Shin[4], Benjamin W Barr[5] , Hyodae Seo[5,6], Dong-Hyun Cha[7] , Min-Ho Kwon[8], Daehyun Kim[9,10] , Moon-Soo Park[11] , Kwang-Young Jeong[12] and Baek-Min Kim[2,*]

[1] APEC Climate Center, Busan 48058, Republic of Korea
[2] Division of Earth Environmental System Science Major of Environmental Atmospheric Sciences, Pukyong National University, Busan 48513, Republic of Korea
[3] Department of Earth, Ocean and Atmospheric Science, Florida State University, Tallahassee, FL 32306, United States of America
[4] Center for Ocean-Atmospheric Prediction Studies, Florida State University, Tallahassee, FL 32306, United States of America
[5] Department of Physical Oceanography, Woods Hole Oceanographic Institution, Woods Hole, MA 02543, United States of America
[6] Department of Oceanography, University of Hawai'i at Mānoa, Honolulu, HI 96822, United States of America
[7] Department of Urban and Environmental Engineering, Ulsan National Institute of Science and Technology, Ulsan 44919, Republic of Korea
[8] Ocean Climate Prediction Center, Korea Institute of Ocean Science and Technology, Busan 49111, Republic of Korea
[9] School of Earth and Environmental Sciences, Seoul National University, Seoul 08826, Republic of Korea
[10] Department of Atmospheric and Climate Science, University of Washington, Seattle, WA 98195, United States of America
[11] Department of Climate and Environment, Sejong University, Seoul 05006, Republic of Korea
[12] Ocean Research Division, Korea Hydrographic and Oceanographic Agency, Busan 49111, Republic of Korea
[*] Author to whom any correspondence should be addressed.

E-mail: baekmin@pknu.ac.kr

Abstract

This study investigates the impact of sea spray parameterization on typhoon prediction in the Yellow and East China Seas (YECS) region. Using an air-sea-wave coupled model, we evaluate changes due to sea spray effects in the simulated intensity and structure of Typhoons Lingling (2019) and Maysak (2020). Enabling sea spray effect enhances surface turbulent heat fluxes considerably around the typhoon centers (74% increase for Lingling, 92% for Maysak), leading to a better representation of typhoon intensification phases. Analysis of thermodynamic processes reveals that sea spray-induced warming emerges before rapid intensification, with enhanced temperature and moisture profiles throughout the troposphere supporting stronger secondary circulation. As a result, key aspects of typhoon prediction exhibit significant improvements: root-mean-squared errors decreased by 63% in minimum central pressure and 60% for maximum wind speed in the case of Maysak. The results demonstrate that sea spray effects are strongly modulated by sub-surface ocean conditions, with a greater surface heat flux enhancement for Maysak that moved along warmer Kuroshio and Tsushima currents than for Lingling which passed over Yellow Sea Bottom Cold Water. Our findings demonstrate the significant potential to improve typhoon predictions in the YECS region by incorporating sea spray effects.

1. Introduction

Accurate typhoon prediction is crucial for mitigating the devastating impacts of powerful typhoons on coastal communities and economies. Despite decades of research (Black *et al* 2007, Rogers *et al* 2013, DeMaria *et al* 2014, Alaka *et al* 2020, 2022, Hazelton *et al* 2023), current typhoon prediction models still

struggle to accurately reproduce observed typhoon intensities (Sroka and Emanuel 2021, Emanuel *et al* 2023). This gap highlights the need for better understanding of air-sea interactions during typhoon prediction. Predicting the rapid intensification of typhoons is particularly challenging, as the role of sea spray—the exchange of heat and moisture above the sea surface by droplets ejected from breaking waves—is often overlooked in recent operational models (DeMaria *et al* 2014, Alaka *et al* 2022, Hazelton *et al* 2023).

Significant progress in formulating spray-mediated heat fluxes has been made through experimental and theoretical studies. Key contributions from laboratory and idealized studies (Andreas 1992, Fairall *et al* 1994, 2009, Andreas and Emanuel 2001, Bao *et al* 2011, Troitskaya *et al* 2017, 2018, Sroka and Emanuel 2021) have refined our understanding of how sea spray influences the energy exchange processes at the air-sea interface. Sea spray also affects sea surface drag coefficients, thereby modifying the air-sea interaction (Andreas 2004, Andreas *et al* 2012, Liu *et al* 2012, Richter and Sullivan 2013, Zhang *et al* 2021). Andreas and colleagues have developed a fundamental framework for parameterizing sea spray fluxes (Andreas 2003, Andreas *et al* 2008, 2015).

Recent studies have demonstrated the potential of incorporating sea spray effects to enhance typhoon intensity predictions. For instance, Xu *et al* (2022) reported a 30% improvement in maximum wind speed predictions when sea spray effects were included in their models. Similarly, Wada *et al* (2018) found that considering sea spray led to a more realistic representation of typhoon rapid intensification phases. A recent study by Yang *et al* (2024) has shed new light on the critical role of sea spray in hurricane intensification. Their research, focused on the Atlantic basin, demonstrated that incorporating sea spray processes, particularly spray-mediated sensible heat flux, significantly improved the accuracy of hurricane intensity predictions. By conducting sensitivity experiments with heat flux parameterizations, they found that including and varying the spray-mediated sensible heat flux substantially reduced model errors when compared against dropsonde data. This paper highlights the important role of sea spray in turbulent heat exchange that drives rapid hurricane intensification. These findings, along with the comprehensive results from Yang *et al* (2024, hereafter YK24), underscore the importance of incorporating sea spray processes in typhoon prediction.

The western North Pacific basin, particularly the Yellow and East China Seas (YECS) region, presents unique challenges for typhoon prediction due to its distinct geographical and oceanographic features compared to the Gulf of Mexico where YK24 conducted their study. While the Gulf of Mexico is characterized by deep waters (>1000 m) and relatively uniform temperature structure dominated by the Loop Current System (Alvera-Azcárate *et al* 2009), the YECS is characterized by shallow depth (<100 m in the Yellow Sea) and a pronounced summer thermocline (Hu *et al* 2024). Additionally, the presence of bottom cold water masses (BCW; He *et al* 1959, Guan 1963) in the YECS region poses significant challenges for simulating typhoons using air-sea coupled models (Moon and Kwon 2012, Ha *et al* 2019, Liu *et al* 2022, Yang *et al* 2022). When a typhoon encounters this bottom cold water mass, it can generate strong temperature horizontal gradients at the sea surface, contributing to the formation of a steeper atmospheric frontal zone (Yang *et al* 2022).

While previous studies have examined typhoon prediction in the YECS region (Moon *et al* 2010, Bae *et al* 2022, Yang *et al* 2022), they have not fully explored the combined effects of sea spray and unique oceanographic features of this area. Although YK24 demonstrated sea spray's importance in hurricane intensity prediction, their findings were based on cases in the Gulf of Mexico where strong ocean currents like the loop current and warm core eddies dominate the upper ocean thermal structure. In contrast, the YECS region is characterized by complex coastal dynamics, including tidal mixing (Lin *et al* 2020), river discharge (Lie *et al* 2003), and seasonal variation of Kuroshio branch currents (Wei *et al* 2015). The shallow waters are also strongly influenced by tide-induced mixing and seasonal stratification (Lee and Beardsley 1999, Xia *et al* 2006), which have shown significant changes in recent decades (Liu *et al* 2021), creating a fundamentally different environment for typhoon-ocean interaction.

The primary hypothesis of our study is that including sea spray in numerical models can significantly improve the accuracy of typhoon intensity predictions in the YECS region, similar to the improvements observed by YK24 in the Atlantic basin. To test this hypothesis, we employ an air-sea coupled model implemented by YK24, incorporating the same sea spray parameterization to reproduce two strong typhoons: Lingling (2019) and Maysak (2020). These typhoons were chosen for their contrasting paths through the YECS region, providing diverse case studies to examine sea spray effects under different oceanic conditions. Lingling moved northward into the Yellow Sea Bottom Cold Water, while Maysak followed the warmer Kuroshio and Tsushima currents.

Therefore, our study aims to quantitatively evaluate sea spray's potential impacts, enhance our understanding of typhoon prediction skills in the YECS region, and examine the role of sea surface conditions in modulating these impacts in numerical simulations. Through case studies of two contrasting typhoons (Lingling and Maysak) in the YECS region, we demonstrate significant improvements in the simulated typhoon intensity and structure when sea spray effects are included. Building upon the work of YK24, we seek to bridge the gap between theoretical

advancements in sea spray physics and their practical application in regional typhoon prediction models, potentially leading to improved forecasting capabilities in the YECS region.

2. Materials and methods

2.1. Overview of typhoons Lingling (2019) and Maysak (2020)

We selected two strong typhoons Lingling and Maysak that recently passed over the YECS region (see colored trajectories in figure 1). Table 1 provides a summary of key characteristics for both typhoons, including their categories, lowest pressure, highest wind speeds, and significant dates. These typhoons passed through the YECS region, and experienced significant sea surface cooling due to typhoon-ocean interactions. We used the Joint Typhoon Warning Center (JTWC) best track data, which provides 6 h observations of typhoon position, intensity, and structure, to verify our model simulations. By classifications in the JTWC data according to 1min sustained maximum wind speed (V_{max}), Lingling and Maysak are both typhoons with a peak V_{max} of 61.1 m s^{-1} (see table 1). These peak intensities are approximately equivalent to Category 4 hurricanes on the Saffir-Simpson Hurricane Wind Scale. They are good examples for understanding the sea spray effects over the bottom cold water mass. Lingling moved northward through the Yellow Sea, while Maysak followed a more eastward track along the Kuroshio and Tsushima currents towards the Korea Strait. These contrasting paths provide diverse case studies for examining sea spray effects under different oceanic conditions.

2.2. Model descriptions

We utilize the Coupled Ocean-Atmosphere-Wave-Sediment Transport (COAWST) modeling system (Warner *et al* 2010), composed of various community models interfaced through the Model Coupling Toolkit (MCT) (Larson *et al* 2005). Our study employs Weather Research and Forecasting (WRF) (Skamarock *et al* 2019) for the atmospheric component, the Regional Ocean Model System (ROMS) (Haidvogel *et al* 2008, Shchepetkin and McWilliams 2009) for the ocean component, and the WAVEWATCH-III (WW3) (WAVEWATCH III Development Group 2016) for the wave component. First, WRF consists of a single domain with a horizontal resolution of 6 km (figure 1), with physics schemes of the WRF Single-Moment 6-class microphysics (Hong and Lim 2006), the Korean Integrated Model Simplified Arakawa-Schubert cumulus (Kwon and Hong 2017), the New Simplified Arakawa-Schubert shallow cumulus (Han and Pan 2011), the Shin-Hong scale-aware planetary boundary layer (Shin and Hong 2013), and the revised MM5 surface layer schemes (Jiménez *et al* 2012). The spatial

domain in WRF is the same as that in ROMS and WW3. Second, ROMS utilizes 3rd-order upstream horizontal advection, 4th-order centered vertical advection, and Mellor-Yamada 2.5 turbulence closure schemes. We employ a double stretching function (Shchepetkin and McWilliams 2009) to define the 32 vertical levels. Third, WW3 explicitly solves directional wave spectra, accounting for whitecap dissipation, nonlinear wave interactions, and wave breaking. We configured a spectral domain with resolutions of 24 frequency and 25 direction bins. The coupling between these MCT, which handles the exchange variables (Warner *et al* 2010). For instance, WRF provides atmospheric parameters such as surface wind stresses to ROMS and WW3, while ROMS feeds back sea surface temperatures (SST) to WRF. WW3 supplies wave parameters to both WRF and ROMS, crucial for accurately representing sea spray effects and wave-induced mixing.

2.3. Sea spray parameterization

Following Andreas's previous research works (Andreas and Decosmo 1999, 2002), the total latent and sensible heat fluxes ($H_{L,T}$ and $H_{S,T}$) in a numerical model can be partitioned as

$$H_{L,T} = H_{L,int} + \alpha Q_L \qquad (1)$$
$$H_{S,T} = H_{S,int} + \beta Q_S - (\alpha - \gamma) Q_L \qquad (2)$$

where $H_{L,int}$ and $H_{S,int}$ are the conventional interfacial latent and sensible heat fluxes, and α, β, and γ are nondimensional, non-negative parameters. We adopt the values of 2.46, 15.15, and 1.77 for these parameters, respectively, as proposed by Andreas *et al* (2015). This choice is supported by YK24, which showed these parameters minimize errors in maximum surface wind speed for intense hurricane cases when compared with high-resolution dropsonde data. Spray latent and sensible heat fluxes (Q_L and Q_S) are defined as $S_a W \Lambda (H_s) H_s B (T_a) \rho_a L_v [q_s (T_a) - q]$ and $S_v W \Lambda (H_s) \rho_w c_{pw} (T_s - T_a)$, respectively, as described by Fairall *et al* (1994). Theses formulations are suitable for wave-coupled simulations. Here, W is the whitecap areal fraction, H_s is significant wave height, ρ_a is the air density, ρ_w is the seawater density, L_v is the latent heat of vaporization of water, c_{pw} is the specific heat of seawater, $B (T_a)$ and $\Lambda (h)$ are the correction factors, S_a is the moisture flux-related parameter of 0.125 s^{-1}, S_v is the relevant whitecap normalized droplet volume flux of 5.0×10^{-6} m s^{-1}, $T_s - T_a$ is the air-sea temperature difference, q_s is the saturation specific humidity, and q is the specific humidity. We also incorporated the wave state-dependent roughness length (z_0) defined as Drennan *et al* (2003):

$$z_0 = 3.35 H_s \left(\frac{u_*}{c_p} \right)^{3.4}. \qquad (3)$$

Here, T_p is peak wave period, L_p is peak wavelength, u_* is frictional velocity, and c_p is phase

Figure 1. Spatial domain of simulation with best tracks for Typhoons Lingling and Maysak. Shaded areas are bathymetry from ETOPO1. The Yellow and East China Seas (YECS) region, characterized by shallow waters and complex oceanographic features, is depicted by the green color box. Starting and dissipated positions of the simulation are marked with circle and cross symbols, respectively, annotated with typhoon names and corresponding dates (dd/mm/yy format), respectively. Typhoon tracks (solid colored lines) are from JTWC best-track data.
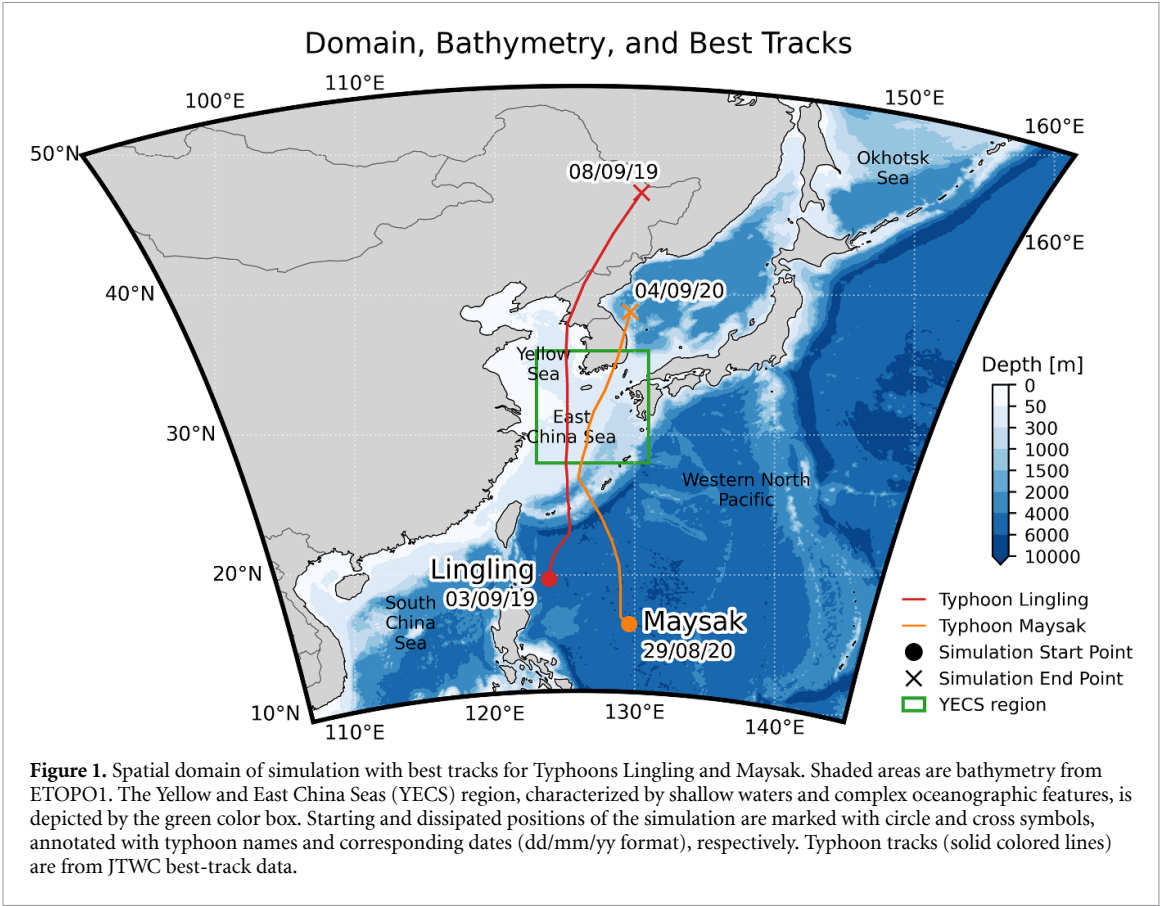
Table 1. A list of case descriptions for typhoons. The peak intensity values of the lowest pressure and highest wind are from the JTWC best-track data.

Typhoon	Category	Lowest pressure (hPa)	Highest wind ($m\ s^{-1}$)	Formed time	Landfall time	Dissipated time	Forecast initialization time
Lingling	Typhoon	928	61.1	00 UTC, 31 August 2019	05 UTC, 4 September 2019	00 UTC, 8 September 2019	00 UTC, 3 September 2019
Maysak	Typhoon	930	61.1	00 UTC, 27 August 2020	17 UTC, 2 September 2020	06 UTC, 3 September 2020	00 UTC, 29 August 2020

speed at spectral peak ($c_p = L_p/T_p$). This formulation accounts for effects of wave age (c_p/u_*) on sea surface roughness (z_0), crucial for accurately representing air-sea momentum transfer in high wind conditions. It complements the sea spray parametrization, enhancing the physical realism of typhoon-ocean-wave interactions in our simulations. These all modifications were applied to the surface layer scheme (Jiménez *et al* 2012) of the WRF model in the COAWST system. The wave parameters (H_s, T_p, L_p, and W) are provided to WRF from WW3.

2.4. Experimental designs

We set up two numerical experiments for each typhoon, CTRL and SPRAY. CTRL is an air-sea coupled simulation using WRF and ROMS (i.e. without sea spray), SPRAY extends this configuration by additionally coupling WW3 to WRF to incorporate sea spray effects, maintaining the same

WRF-ROMS coupling. Note that wave-current interactions are excluded as WW3 and ROMS are not directly coupled.

Both simulations were run for 120 h, excluding the first 24 h as a spin-up period. While using identical initial and boundary conditions, SPRAY incorporates additional heat and momentum fluxes induced by sea spray, potentially altering air-sea interaction and subsequent typhoon development.

WRF is initialized at specified times (table 1) using ERA5 reanalysis data (Hersbach *et al* 2020) with 25 km horizontal resolution, providing hourly updates of lateral boundary conditions. Spectral nudging (SN) toward large-scale flow was applied to reduce track biases (Li *et al* 2021). ROMS integrates eight tidal constituents (Q1, O1, P1, K1, N2, M2, S2, and K2) from TPXO8-atlas (Egbert and Erofeeva 2002) at open boundaries. Initial and lateral boundary conditions provided by the Hybrid

Coordinate Ocean Model (HYCOM) (Cummings 2006) with a spatial resolution of 0.08° longitude × 0.04° latitude covering 80°S to 90°N, updated daily. Bathymetry is based on the 1 Min Gridded Global Relief Data. For WW3, we have modified the COAWST to transfer whitecap areal fraction from the ST4 dissipation package (Ardhuin *et al* 2010) to WRF via MCT for calculating spray heat fluxes through equations (1) and (2). Components exchange variables every 10 min.

To detect typhoons and subsequently track their centers based on simulation results, we employed the Geophysical Fluid Dynamics Laboratory (GFDL) vortex tracker (Biswas *et al* 2018). In particular, we decomposed the horizontal velocity field $\mathbf{V} = (u, v)$, relative to the typhoon central positions (x_0, y_0) into radial (v_r) and tangential (v_θ) components as follows:

$$v_r = \mathbf{V} \cdot \hat{\mathbf{r}} = u\cos\theta + v\sin\theta, \; v_\theta = \mathbf{V} \cdot \hat{\boldsymbol{\theta}}$$
$$= -u\sin\theta + v\cos\theta, \tag{4}$$

where $\theta = \operatorname{atan2}(y - y_0, x - x_0)$, $\hat{\mathbf{r}}$ is the radial unit vector, and $\hat{\boldsymbol{\theta}}$ is the tangential unit vector. This decomposition enables us to better characterize the radial inflow and tangential wind structure of the typhoon.

Typhoon size can be determined in various ways (Knaff *et al* 2016). The JTWC best track data provides quadrant-specific 34 kt wind radii (NE, SE, SW, and NW) and the radius of maximum wind (RMW). For our model simulations, we utilized the GFDL vortex tracker (Biswas *et al* 2018) to extract these same structural parameters. For both our model simulations and JTWC best track data, we define R34$_{avg}$ as the average of the four quadrant-specific 34 kt wind radii, which represents the outer-core boundary (i.e. the tropical storm force limit) at each forecast time step. The inner core is defined as the region extending 4 times the RMW from the typhoon center.

3. Results

3.1. Initial ocean conditions in YECS
The initial ocean conditions in the YECS region play a crucial role in typhoon development and intensification. Figure 2 illustrates the horizontal distribution of SST and subsurface temperature at a depth of 45 m, representing the BCW, from the HYCOM initial conditions for typhoons Lingling and Maysak.

For Lingling, we observe a clear stratification in the YECS region (figures 2(a)–(c)). The SST shows relatively warm waters, with temperatures ranging from 26 °C to 30 °C across most of the area (figure 2(a)). However, the subsurface reveals colder water masses, particularly in the Yellow Sea, with temperatures as low as 10 °C–14 °C (figure 2(b)). These results in a significant temperature difference between BCW and SST, exceeding −12 °C in some Yellow Sea areas (figure 2(c)).

For Maysak, the initial conditions show some differences (figures 2(d)–(f)). The SST distribution is similar to Lingling, but with slightly colder temperatures in the northern Yellow Sea (figure 2(d)). This cooling can be attributed to Typhoon Bavi's (2020) passage a few days prior, as noted by Hong *et al* (2022) who observed post-Bavi SST decreases of up to 8 °C. The subsurface temperature shows a similar pattern to Lingling, but with a slightly larger extent of colder waters (figure 2(e)). The temperature difference between BCW and SST ranges from −6 °C to −2 °C in the East China Sea and exceeding −10 °C in parts of the Yellow Sea (figure 2(f)).

These features have important implications for typhoon development. As Lingling moves northward into the Yellow Sea, it encounters strong sea surface cooling due to BCW upwelling (Yang *et al* 2022). In contrast, Maysak's path along the Kuroshio and Tsushima currents is characterized by warmer SSTs above 26 °C, potentially supporting intensification. These conditions highlight the significant thermocline and BCW presence in the region.

3.2. Typhoon intensity and structure
Sea spray incorporation significantly improved typhoon intensity and structure predictions for both Lingling and Maysak. Figure 3 shows reduced mean bias errors (MBEs) for minimum central pressure (P_{min}) and maximum wind speed (V_{max}) in SPRAY compared to CTRL. For P_{min}, SPRAY showed lower MBEs, particularly for Maysak with $\sim 76\%$ reduction using SN. V_{max} predictions improved notably for Lingling with SN reduced position errors by 23 km for Lingling and 35 km for Maysak. The minimal impact of sea spray on position errors indicates track accuracy depends large-scale flow features, while local air-sea interaction processes influence intensity. Furthermore, sea spray improved typhoon size prediction, with R34$_{avg}$ MBEs decreasing from 33.3 km to 21.1 km for Lingling (36.5%) and from 151.3–126.1 km for Maysak (16.7%), correcting the overestimation tendency observed in CTRL simulations.

Time series analysis shows that SPRAY better captured typhoon intensity evolution compared to CTRL (figure 4). SPRAY systematically reduces intensity biases in P_{min} and V_{max} throughout the forecast period, with the largest corrections occurring during 24 h peak stages (36–60 h for Lingling, 49–72 h for Maysak) and better alignment with JTWC best-track data. These improvements reduced root-mean squared error (RMSE) of V_{max} from 20.4 m s^{-1} to 12.5 m s^{-1} for Lingling (38.7% reduction) and from 19.3 m s^{-1} to 7.1 m s^{-1} for Maysak (63.1% reduction). RMSE of P_{min} also decreased by 29.1% for Lingling and 60.1% for Maysak (figures 4(a) and (e)).

Detailed analysis of intensity evolution reveals distinct characteristics for both typhoons. For Lingling, SPRAY captured a peak V_{max} of 44.8 m s^{-1} at 51 h, which is closer to the observed 61.1 m s^{-1}
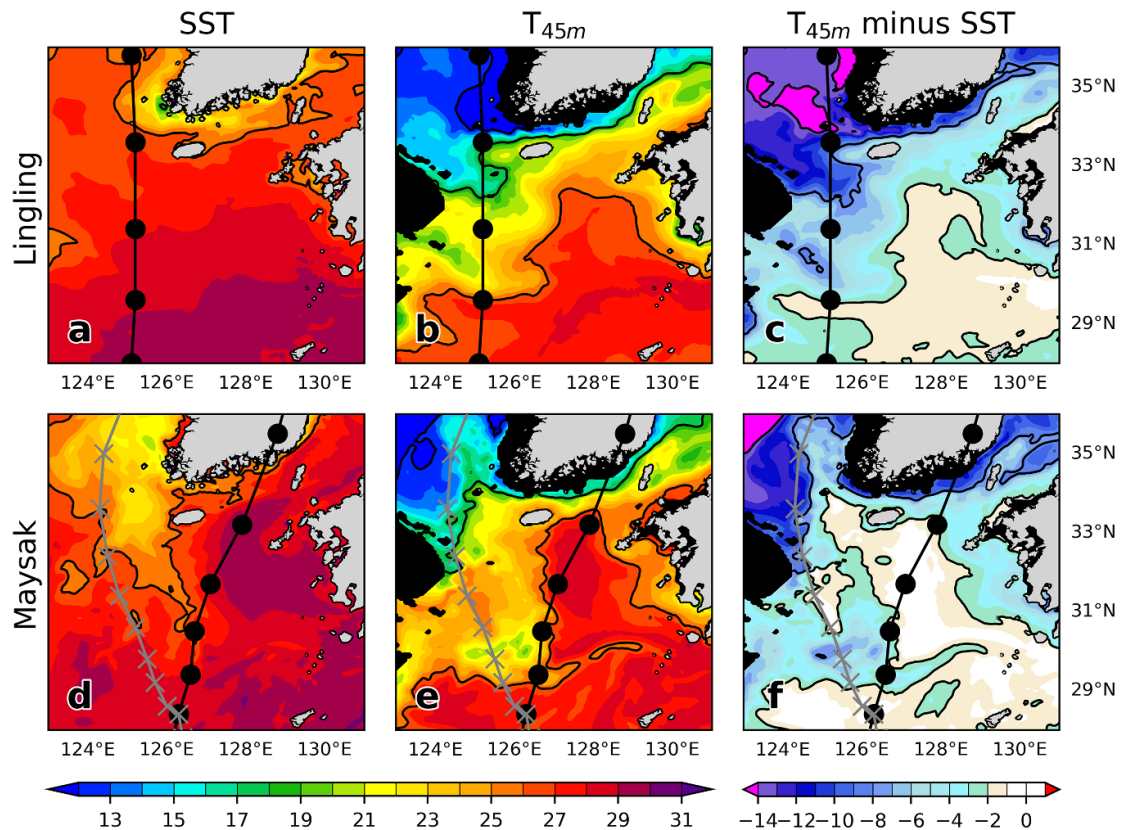
Figure 2. Horizontal distributions of ocean temperatures in the YECS region from HYCOM initial conditions for typhoons
(a)–(c) Lingling (00 UTC, 3 September 2019) and (d)–(f) Maysak (00 UTC, 29 August 2020). (a), (d) Sea surface temperature
(SST), (b), (e) sea subsurface temperature at a depth of 45 m representing bottom cold water (BCW), and (c), (f) temperature
difference between SST and BCW. The shading represent temperature in °C. Black contour lines in (a), (b), (d), (e) indicate
12 °C, 18 °C, and 26 °C isotherms, while in (c), (f) they represent −14 °C, −8 °C, and −2 °C temperature differences. Typhoon
tracks based on JTWC best track data (lines with markers at 6 h intervals) are shown in all panels. In panel (d)–(f), the gray
cross-marked line represents the track of Typhoon Bavi, which preceded Maysak in the YECS region.
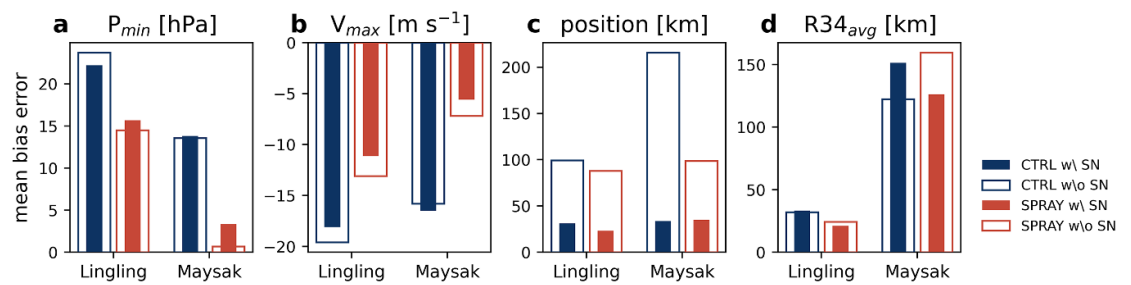

Figure 3. Bar charts of mean bias errors (MBEs) for (a) center minimum pressure (P_{min}), (b) maximum wind speed (V_{max}), (c)
position, and (d) out-core radius (R34$_{avg}$) in CTRL and SPRAY simulations compared to JTWC best track data for typhoons
Lingling and Maysak. The MBEs are computed over the 24–120 h period (the first 24 h are excluded as a spin-up period). All
simulation results are with- and without SN technique displayed by filled- and unfilled bars. Positive (negative) values denote
overestimation (underestimation) against the best track data. Values closer to zero suggest more accurate predictions.

at 54 h, versus CTRL's underestimated 37 m s^{-1} at
87 h (figure 4(b)). For Maysak, SPRAY produced
a peak of 51.4 m s^{-1} at 72 h, matching JTWC's
peak timing, while CTRL reached only 47 m s^{-1}
at 57 h (figure 4(f)). These timing differences high-
light the relationship between wind and pressure
fields. Following Knaff and Zehr (2007), SPRAY
shows more synchronized evolution in wind-pressure
coupling over a 24–120 h period. The P_{min} and

V_{max} correlations are stronger in SPRAY (Lingling:
$r = −0.81$; Maysak: $r = −0.96$) than CTRL (Lingling:
$r = −0.70$; Maysak: $r = −0.77$), all statistically sig-
nificant ($p < 0.01$). These results reflect improved
representation of typhoon size and intensification
trends. The concurrent timing of peak intensities in
SPRAY, compared to CTRL's lagged responses, sug-
gests more physically consistent representation of
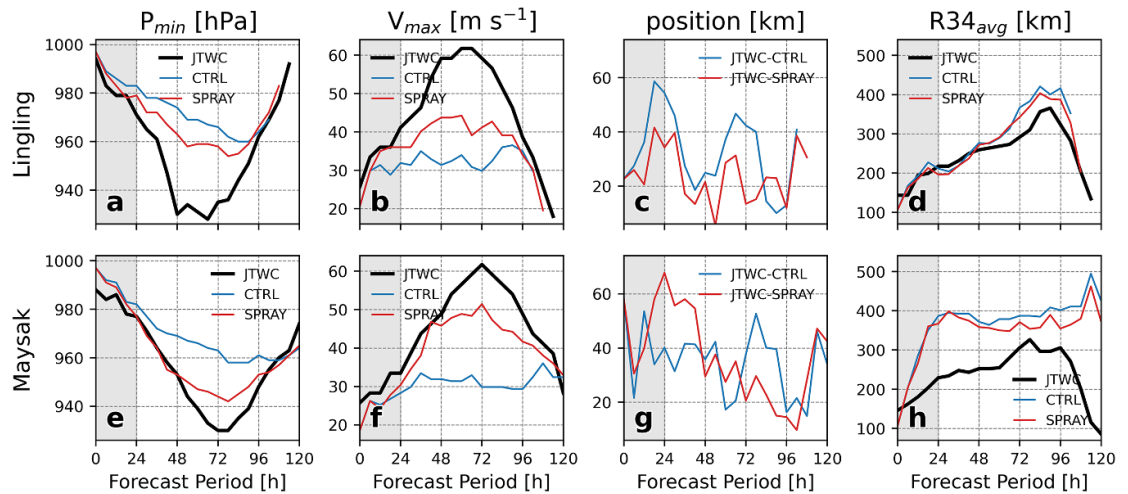intensification processes.

Figure 4. Time series of the (a), (e) center minimum pressure (P_{min}), (b), (f) maximum wind speed (V_{max}), (c), (g) position, and (d), (h) out-core radius ($R34_{avg}$) comparing simulation results with JTWC best track data across Typhoons (top) Lingling and (bottom) Maysak. Data points are presented at 6 h intervals. Gray shading denotes the 24 h spin-up period following each initialization time (see table 1). For each legend, the value in parentheses next to the simulation name represents the root-mean-square error for JTWC best track data.
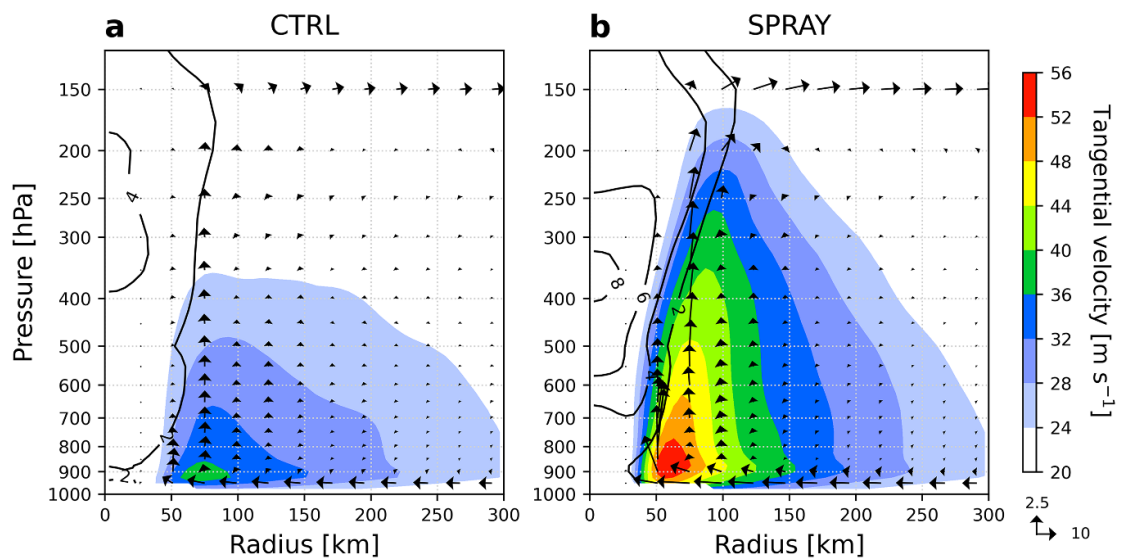

Figure 5. Radius-pressure cross-sections of azimuthally and temporally averaged structure of Typhoon Maysak during the 24 h peak stage (49–72 h; see typhoon intensity changes in figure 4(f)) for (a) CTRL and (b) SPRAY simulations. Shading represents tangential velocity (m s^{-1}). Vectors indicate radial velocity (m s^{-1}) and vertical velocity (Pa s^{-1}), with the scale shown in the bottom right corner. Contours show potential temperature anomalies [K], defined as deviations from the radial mean.
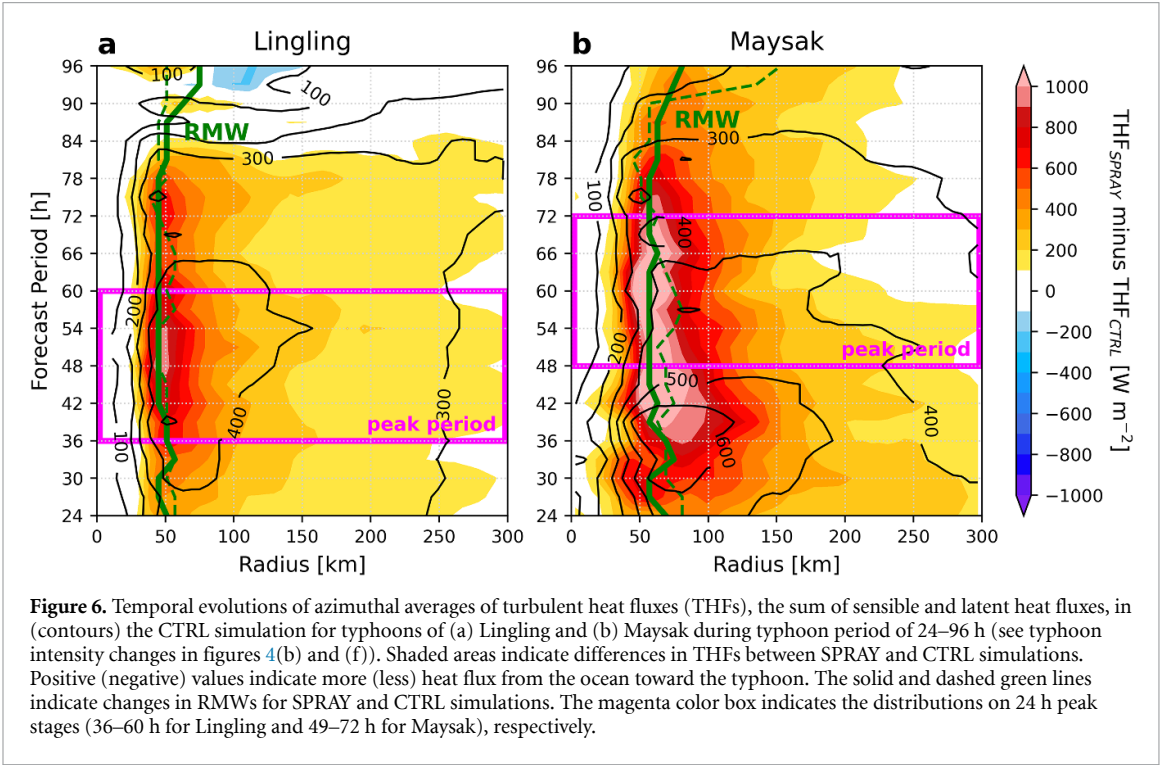
SPRAY maintained higher intensities during the peak stages (figures 4(a), (b) and (f), (g)). While air-sea interactions typically produce negative SST feedback through surface cooling (Price 1981, Schade and Emanuel 1999, Lin *et al* 2008, Mogensen *et al* 2017), sea spray incorporation better captures temporal evolution and peak intensity.

For both typhoons, CTRL and SPRAY show similar track evolution due to the use of SN (figures 4(c) and (g)). In terms of structural characteristics, SPRAY reduces the overestimation of $R34_{avg}$ in CTRL throughout the forecast period, with biases decreasing for both cases (figures 4(d) and (h)).

Figure 5 compares Maysak's the azimuthally averaged structure during peak stages. SPRAY produced stronger tangential winds in the eyewall, extending to higher with small RMW. These changes indicate more intense and better-organized structure. The secondary circulation showed stronger low-level inflow and upper-level outflow. This low-level convergence relative to RMW indicates intensity change (Ahern *et al* 2021, 2022), suggesting enhanced secondary circulation drives intensification. Vertical motion and warm core extended to higher, indicating vigorous convection and efficient energy conversion. Similar enhancements appeared in Lingling's case.

Table 2. Comparison of key variables between CTRL and SPRAY simulations for typhoons Lingling and Maysak. Values shown are from SPRAY simulations, averaged within a 300 km radius from the typhoon center during 24 h peak stages (36–60 h for Lingling, 49–72 h for Maysak). Negative radial velocity at 925 hPa indicates inflow towards the typhoon center. Positive vertical velocity at 500 hPa indicates upward motion. Percentages in parentheses indicate the relative differences from CTRL, calculated as (SPRAY-CTRL)/CTRL × 100.

Key variables	Typhoons	
	Lingling	Maysak
Turbulent heat flux	589.24 W m^{-2} (+73.81%)	671.63 W m^{-2} (+92.19%)
Tangential velocity at 850 hPa	26.25 m s^{-1} (+10.22%)	32.85 m s^{-1} (+20.95%)
Radial velocity at 925 hPa	-4.77 m s^{-1} (+119.03%)	-7.64 m s^{-1} (+111.89%)
Radial velocity at 150 hPa	6.37 m s^{-1} (+14.47%)	7.68 m s^{-1} (+82.78%)
Vertical velocity (-omega) at 500 hPa	0.80 Pa s^{-1} (+39.11%)	0.74 Pa s^{-1} (+73.63%)

Figure 6. Temporal evolutions of azimuthal averages of turbulent heat fluxes (THFs), the sum of sensible and latent heat fluxes, in (contours) the CTRL simulation for typhoons of (a) Lingling and (b) Maysak during typhoon period of 24–96 h (see typhoon intensity changes in figures 4(b) and (f)). Shaded areas indicate differences in THFs between SPRAY and CTRL simulations. Positive (negative) values indicate more (less) heat flux from the ocean toward the typhoon. The solid and dashed green lines indicate changes in RMWs for SPRAY and CTRL simulations. The magenta color box indicates the distributions on 24 h peak stages (36–60 h for Lingling and 49–72 h for Maysak), respectively.

These results collectively demonstrate sea spray parameterization enhances typhoon prediction accuracy across multiple metrics in the YECS region.

3.3. Factors modulating typhoon intensification
Our analysis reveals key factors modulating typhoon intensification in the YECS region, with sea spray playing a crucial role.

Table 2 compares key factors between CTRL and SPRAY during peak stages for both typhoons. The most significant differences appeared in turbulent heat flux and low-level inflow. The turbulent heat flux increases by 74% for Lingling and 92% for Maysak in SPRAY, reflecting both direct sea spray effects and feedback from stronger surface winds. The low-level inflow at 925 hPa shows increases of 115% for Lingling and 112% for Maysak. This enhanced inflow and increased upper-level outflow indicates stronger secondary circulation, improving typhoon structure and intensity representation.

Figure 6 shows temporal evolution of turbulent heat fluxes (THFs) over 24–96 h, providing insight

into sea spray's influence on intensification. SPRAY exhibits enhanced THFs during peak stages for both typhoons, most pronounced within 100 km of the center. RMW contraction correlates with enhanced THFs, suggesting increased heat and moisture transfer creates a more compact and intense structure.

To further explain the impact of sea spray on the thermodynamic structures of typhoons, we examined the vertical distributions of differences in potential temperature (θ), equivalent potential temperature (θe), and mixing ratio (mr) between SPRAY and CTRL during the peak stage of Typhoon Maysak (figure 7). The θ distribution indicates an increase of 1–2 K within the boundary layer ($<$900 hPa) and 3–4 K in the upper-level outflow region ($>$300 hPa), with particularly pronounced warming of 5 K in the upper-level core (figure 7(a)). The θe distribution indicates warming of 6 K in the upper troposphere along the eyewall updraft that is indicative of intensified latent heat release (figure 7(b)). Concurrently, the mr distribution reveals a positive difference of approximately 2 g kg^{-1} along the eyewall updraft
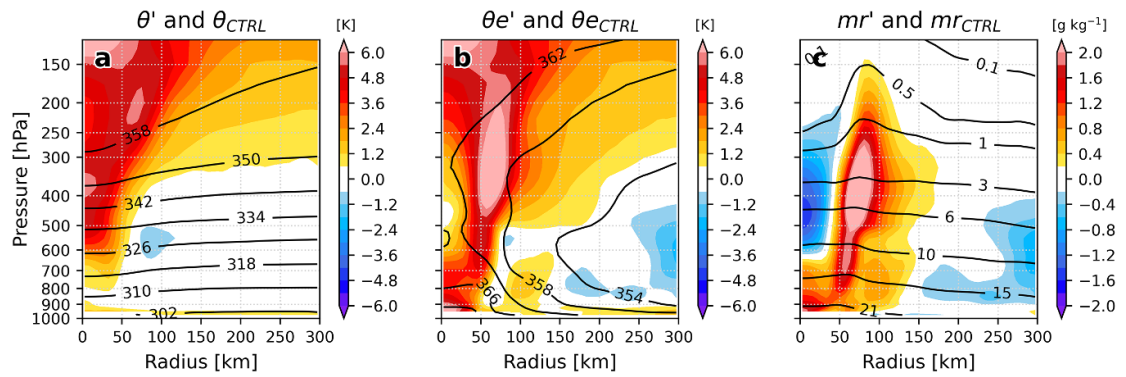
Figure 7. Radius-pressure cross-sections of azimuthally and temporally averaged (a) potential temperature (θ), (b) equivalent potential temperature (θe), and (c) mixing ratio (mr) of Typhoon Maysak during the peak stage (49–72 h). Shading indicates differences between SPRAY and CTRL simulations (prime denotes SPRAY minus CTRL), while contours show the CTRL distribution.
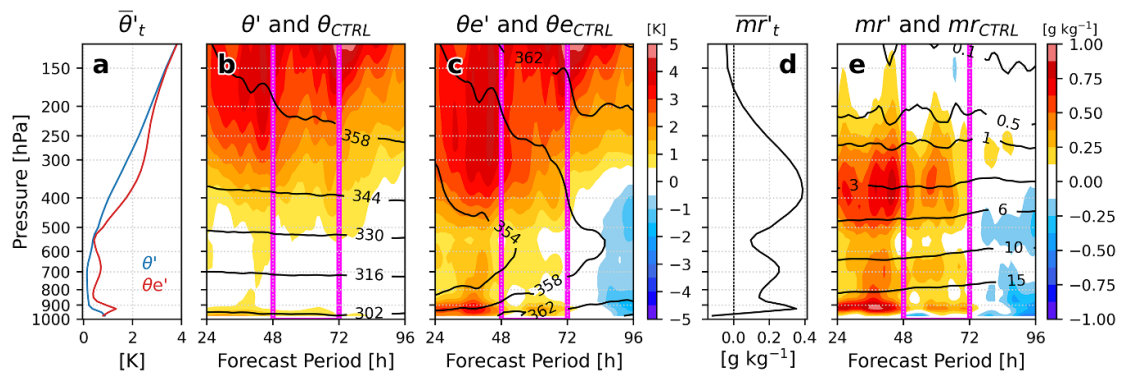

Figure 8. Radius-pressure cross-sections of azimuthally and radially averaged potential temperature (θ), equivalent potential temperature (θe), and mixing ratio (mr) of Typhoon Maysak within a 300 km radius from the typhoon center. (a) Vertical profiles of averaged θ 'and θe 'during the peak stage (49–72 h). (b), (c) temporal evolution of θ 'and θe'. (d) Similar to (a) but for mr'. (e) Temporal evolution of mr'. Shading indicates differences between SPRAY and CTRL simulations (prime denotes SPRAY minus CTRL), while contours show the CTRL distribution.
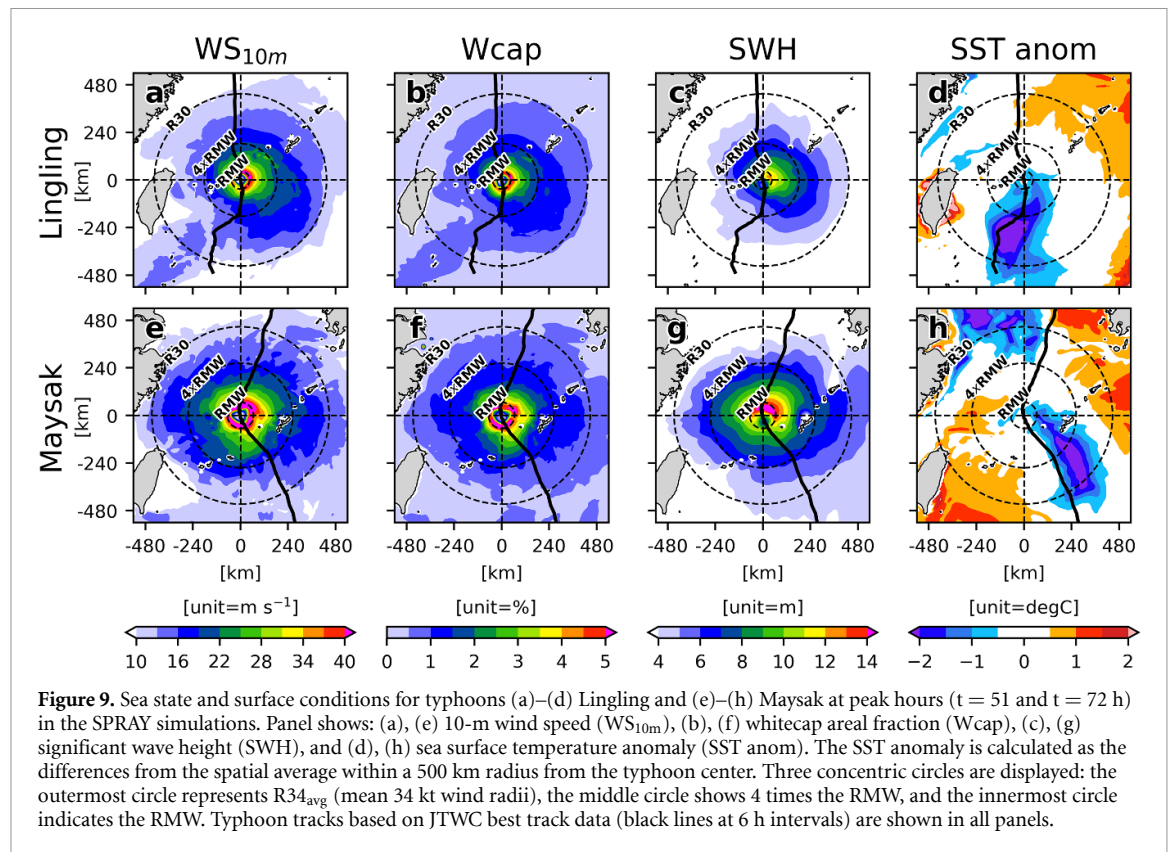
across the vertical extent of the typhoon, underscoring the moisture enhancement associated with sea spray from the near-surface to the upper troposphere (figure 7(c)).

The vertical profiles and their temporal evolution demonstrate that this warming emerges before the onset of rapid intensification at 48 h (figure 8). The vertical stability characteristics through θ and θe anomalies reveal modified thermal stratification under sea spray effects (figure 8(a)). The upper-level warming shows a 3 K increase at 250 hPa, approximately twice the magnitude at lower levels (1 K at 950 hPa). The temporal evolution of θ 'and θe 'indicates that reduced static stability and enhanced convective instability initiate before the peak stage (figures 8(b) and (c)). This vertical redistribution of warming represents a preconditioning mechanism that enhanced thermal efficiency within the system. Sustained positive mr 'of 0.5 g kg^{-1} through most of the troposphere over a 24–72 h period provide conditions favorable for deep convection (figures 8(d) and (e)). Similar but more moderate modifications were

found in Lingling. Collectively, these findings underscore how sea spray–induced enhancements in air-sea heat and moisture exchange sustain a stronger secondary circulation.

To better demonstrate these complex typhoon-ocean interactions, we have provided supplementary video animations. Videos S1 (SPRAY) and S2 (CTRL) for Typhoon Lingling, and videos S3 (SPRAY) and S4 (CTRL) for Typhoon Maysak visualize the temporal evolution of key processes including typhoon structure development, secondary circulation patterns, and ocean temperature responses. These animations strengthen our findings by clearly showing the enhanced typhoon development in SPRAY compared to CTRL.

Figure 9 illustrates sea state and surface conditions at peak intensity, showing the SPRAY results only as CTRL consistently exhibited weaker intensities. The 10 m wind speed distribution shows the classic typhoon structure, with strongest winds within the RMW (figures 9(a) and (e)), reaching 51.03 m s^{-1} for Maysak and 43.81 m s^{-1}

Figure 9. Sea state and surface conditions for typhoons (a)–(d) Lingling and (e)–(h) Maysak at peak hours (t = 51 and t = 72 h) in the SPRAY simulations. Panel shows: (a), (e) 10-m wind speed (WS$_{10m}$), (b), (f) whitecap areal fraction (Wcap), (c), (g) significant wave height (SWH), and (d), (h) sea surface temperature anomaly (SST anom). The SST anomaly is calculated as the differences from the spatial average within a 500 km radius from the typhoon center. Three concentric circles are displayed: the outermost circle represents R34$_{avg}$ (mean 34 kt wind radii), the middle circle shows 4 times the RMW, and the innermost circle indicates the RMW. Typhoon tracks based on JTWC best track data (black lines at 6 h intervals) are shown in all panels.

for Lingling (72% and 27% higher than CTRL). Whitecap areal fraction correlates with wind speed in high-wind areas, with maximum values of 6.3% and 5.29%, indicating increased spray flux, Q_L and Q_S (figures 9(b) and (f)). Significant wave heights peaks at 15.04 m and 12.28 m in the right-front quadrant, extending beyond the inner-core region (figures 9(c) and (g)). This asymmetry results from both stronger winds and resonant wave growth in the right quadrant, while waves on the left side remain unaligned and grow less effectively. This pattern has been well-documented in previous studies (e.g. Barr *et al* 2023). SST anomalies show cooling in the wake of both typhoons, with the coldest anomalies of $-2.62\,°C$ and $-3.39\,°C$ (58% and 20% colder than CTRL) typically found on the right side of the track, often extending beyond R34$_{avg}$ (figures 9(d) and (h)). This cooling is due to typhoon-induced mixing bringing cooler subsurface water upward (Price 1981, D'Asaro *et al* 2007), potentially affecting further intensification.

4. Discussion and conclusions

This study extends the work of YK24 on hurricane prediction in the Atlantic basin to the western Pacific context, demonstrating the significant impact of sea spray parameterization on typhoon prediction in the YECS region. Unlike YK24, this study presents one of the first attempts to integrate a wave-dependent spray parameterization within a fully coupled atmosphere-ocean-wave system for

shallow marginal seas characterized by bottom cold water. We further implemented the wave age-based roughness length parameterization (Drennan *et al* 2003) to better represent wind-wave interactions and the wave field asymmetry observed in our results. Our approach bridges the framework of Atlantic-based studies with the unique oceanographic conditions of the YECS region–notably, shallow bathymetry, strong tidal mixing, and the presence of bottom cold water masses.

For Typhoons and Lingling (2019) and Maysak (2020), the incorporation of sea spray processes substantially improves typhoon intensity and structure predictions. Specifically, sea spray incorporation reduced MBEs and RMSE s in minimum central pressure and maximum wind speed. SPRAY simulations captured a more realistic typhoon structure, with R34$_{avg}$ MBEs decreasing by 37% for Lingling and 17% for Maysak, particularly the compact and intense eyewall region. Enhanced THFs in SPRAY simulations (74% increase for Lingling, 92% for Maysak) led to better representation of intensification phases. These results align with YK24's findings on the critical role of spray-mediated sensible heat flux in accurately predicting rapid intensification.

Analysis of thermodynamic processes reveals that sea spray effects significantly modify the vertical structure of Typhoon Maysak. Potential temperature shows enhanced warming in both the boundary layer (1–2 K) and upper levels (3–4 K), with maximum warming of 5 K in the upper-level core.

These modifications, emerging before rapid intensification at 48 h, feature intensified latent heat release and increased moisture throughout the troposphere. The vertical redistribution of warming and sustained moisture enhancement creates conditions favorable for deep convection, demonstrating how sea spray effects strengthen the secondary circulation through enhanced air-sea exchanges.

Our results extend the theoretical work of Andreas and Emanuel (2001) on spray-mediated enthalpy flux contributions to typhoon intensity. The varying impact of sea spray under different oceanic conditions, as represented in our study, builds upon the work of Chen *et al* (2018) on the relationship between rapid intensification and SST, while exploring these effects in a region with unique oceanographic features such as bottom cold water masses. Notably, the nondimensional parameters ($\alpha = 2.46$, $\beta = 15.15$, and $\gamma = 1.77$) of Andreas *et al* (2015) originally calibrated for low-to-moderate wind conditions have proven effective in reducing forecast errors, although further field validation in coastal environments could help refine theses values.

Despite these advancements, our model shows limitations in predicting peak intensity, partially attributed to the use of constant sea spray generation-related constant parameters (S_a and S_v). The recent work of Barr *et al* (2023) demonstrate that sea spray effects vary significantly with wind speed, suggesting that future work should implement wind- and sea-state dependent sea spray generation functions, such as those proposed by Troitskaya *et al* (2018) and Xu *et al* (2021), to better represent droplet size distribution and its dependencies. Additionally, understanding the combined effects of sea spray with upper-ocean thermal structure (Lin *et al* 2009, Wada *et al* 2009) and internal typhoon dynamics (Smith and Montgomery 2016) could further enhance prediction accuracy.

Similar to YK24, our study demonstrates efficacy for strong typhoons with intense air-sea coupling. However, extending this approach to weaker typhoons is still challenging. Lower wind speeds and less developed wave fields limit sea spray fluxes within these systems, implying that coupling effects may not be as pronounced. This suggests the need for future case studies on marginal or developing typhoons to quantify threshold-based relationships between wind speed, wave state, and sea spray generation. Understanding these relationships represents a critical step toward sea spray effects in various air-sea coupled processes such as marine heat waves and sea fog formation. Our results also highlight the importance of environmental preconditioning of typhoon development, as evidenced by Typhoon Bavi's passage that cooled the ocean and subsequently influenced Typhoon Maysak's evolution.

ERA5 data was selected for its high-resolution and consistent historical coverage, which was ideal for this study. To implement our sea spray parameterization in operational systems like Hurricane Analysis and Forecasting System (Alaka *et al* 2022) with its high-resolution moving nests, we would need to evaluate its performance using different combinations of operational data. For the atmospheric component, global forecast models such as the Global Forecast System and Integrated Forecasting System would provide initial and lateral boundary conditions. For the ocean component, operational analysis products like the HYCOM and Global Ocean Reanalysis System would provide initial states and open boundary conditions. The robustness of the parameterization also needs to be tested across different physics configurations available through the Common Community Physics Package (Bernardet *et al* 2024).

This study underscores the need for enhanced *in situ* flux observations and sea spray measurements using diverse platforms (e.g. dropsonde, fixed ocean towers, and autonomous surface vehicles). The Ieodo Ocean Research Station (I-ORS), strategically located in the path of typhoons approaching the Korean Peninsula (Ha *et al* 2019), has the potential to sample most of the typhoon atmospheric surface layer and ocean mixed layer from a fixed frame of Yang *et al* (2022). Its location on the continental shelf of the Yellow Sea is ideal for measuring typhoon-generated waves without coastal interference. Leveraging its capacity for large equipment and installing additional support structure near the sea surface could enable direct measurements of spray droplet size distribution and air-sea fluxes at the air-sea interface. These advancements would provide critical data for model development, significantly advancing our understanding of air-sea interactions during extreme weather events.

Data availability statement

Acknowledgments

Conflict of interest

The authors declare that they have no conflict of interest.

ORCID iDs

Sinil Yang ⬤ https://orcid.org/0000-0002-8851-6495
Benjamin W Barr ⬤ https://orcid.org/0000-0001-6983-3519
Hyodae Seo ⬤ https://orcid.org/0000-0002-4352-5080
Dong-Hyun Cha ⬤ https://orcid.org/0000-0001-5053-6741
Daehyun Kim ⬤ https://orcid.org/0000-0001-9233-2747
Moon-Soo Park ⬤ https://orcid.org/0000-0003-0551-5129
Baek-Min Kim ⬤ https://orcid.org/0000-0002-1717-183X

References

Ahern K, Hart R E and Bourassa M A 2021 Asymmetric hurricane boundary layer structure during storm decay. Part I: formation of descending inflow *Mon. Weather Rev.* **149** 3851–74

Ahern K, Hart R E and Bourassa M A 2022 Asymmetric hurricane boundary layer structure during storm decay. Part II: secondary eyewall formation *Mon. Weather Rev.* **150** 1915–36

Alaka G J, Sheinin D, Thomas B, Gramer L, Zhang Z, Liu B, Kim H S and Mehra A 2020 A hydrodynamical atmosphere/ocean coupled modeling system for multiple tropical cyclones *Atmosphere* **11** 1–22

Alaka G J, Zhang X and Gopalakrishnan S 2022 High-definition hurricanes: improving forecasts with storm-following nests *Bull. Am. Meteorol. Soc.* **103** E680–703

Alvera-Azcárate A, Barth A and Weisberg R H 2009 The surface circulation of the Caribbean Sea and the Gulf of Mexico as inferred from satellite altimetry *J. Phys. Oceanogr.* **39** 640–57

Andreas E L 1992 Sea spray and the turbulent air-sea heat fluxes *J. Geophys. Res.* **97** 429–41

Andreas E L 2003 An algorithm to predict the turbulent air-sea fluxes in high-wind, spray conditions *Environ. Sci.* 1–7 (available at: http://ams.confex.com/ams/pdfpapers/52221.pdf)

Andreas E L 2004 Spray stress revisited *J. Phys. Oceanogr.* **34** 1429–40

Andreas E L and Decosmo J 1999 *Sea Spray Production and Influence on Air-sea Heat and Moisture Fluxes over the Open Ocean* (Springer)

Andreas E L and Decosmo J 2002 The signature of sea spray in the hexos turbulent heat flux data *Bound.-Layer Meteorol.* **103** 303–33

Andreas E L and Emanuel K A 2001 Effects of sea spray on tropical cyclone intensity *J. Atmos. Sci.* **58** 3741–51

Andreas E L, Mahrt L and Vickers D 2012 A new drag relation for aerodynamically rough flow over the ocean *J. Atmos. Sci.* **69** 2520–37

Andreas E L, Mahrt L and Vickers D 2015 An improved bulk air-sea surface flux algorithm, including spray-mediated transfer *Q. J. R. Meteorol. Soc.* **141** 642–54

Andreas E L, Persson P O G and Hare J E 2008 A bulk turbulent air-sea flux algorithm for high-wind, spray conditions *J. Phys. Oceanogr.* **38** 1581–96

Ardhuin F *et al* 2010 Semiempirical dissipation source functions for ocean waves. Part I: definition, calibration, and validation *J. Phys. Oceanogr.* **40** 1917–41

Bae H J, Yang S, Jeong T B, Yang A R, Cha D H, Lee G, Lee H Y, Byun D S and Kim B M 2022 An estimation of ocean surface heat fluxes during the passage of typhoon at the ieodo ocean research station: typhoon lingling case study 2019 *Asia-Pac. J. Atmos. Sci.* **58** 305–14

Bao J W, Fairall C W, Michelson S A and Bianco L 2011 Parameterizations of sea-spray impact on the air-sea momentum and heat fluxes *Mon. Weather Rev.* **139** 3781–97

Barr B W, Chen S S and Fairall C W 2023 Sea-state-dependent sea spray and air-sea heat fluxes in tropical cyclones: a new parameterization for fully coupled atmosphere-wave-ocean models *J. Atmos. Sci.* **80** 933–60

Bernardet L, Bengtsson L, Reinecke P A, Yang F, Zhang M, Hall K, Doyle J, Martini M, Firl G and Xue L 2024 Common community physics package: fostering collaborative development in physical parameterizations and suites *Bull. Am. Meteorol. Soc.* **105** E1490–505

Biswas M K, Stark D and Carson L 2018 GFDL vortex tracker users guide version 3.9 a (National Center Atmospheric Research Developmental Testbed Center)

Black P G, D'Asaro E A, Drennan W M, French J R, Niiler P P, Sanford T B, Terrill E J, Walsh E J and Zhang J A 2007 Air-sea exchange in hurricanes *Bull. Am. Meteorol. Soc.* **88** 357–74

Chen X, Xue M and Fang J 2018 Rapid intensification of Typhoon Mujigae (2015) under different sea surface temperatures: structural changes leading to rapid intensification *J. Atmos. Sci.* **75** 4313–35

Cummings J A 2006 Operational multivariate ocean data assimilation *Q. J. R. Meteorol. Soc.* **131** 3583–604

D'Asaro E A, Sanford T B, Niiler P P and Terrill E J 2007 Cold wake of Hurricane Frances *Geophys. Res. Lett.* **34** 2–7

DeMaria M, Sampson C R, Knaff J A and Musgrave K D 2014 Is tropical cyclone intensity guidance improving? *Bull. Am. Meteorol. Soc.* **95** 387–98

Drennan W M, Graber H C, Hauser D and Quentin C 2003 On the wave age dependence of wind stress over pure wind seas *J. Geophys. Res.* **108** 1–13

Egbert G D and Erofeeva S Y 2002 Efficient inverse modeling of barotropic ocean tides *J. Atmos. Ocean. Technol.* **19** 183–204

Emanuel K A, Velez-pardo M and Cronin T W 2023 The surprising roles of turbulence in tropical cyclone physics *Atmosphere* **14** 1–14

Fairall C W, Banner M L, Peirson W L, Asher W and Morison R P 2009 Investigation of the physical scaling of sea spray spume droplet production *J. Geophys. Res.* **114** 1–19

Fairall C W, Kepert J D and Holland G J 1994 The effect of sea spray on surface energy transports over the ocean *Glob. Atmos. Ocean Syst.* **2** 121–42

Guan B X 1963 A preliminary study of the temperature variations and the characteristics of the circulation of the cold water mass of the Yellow Sea *Oceanol. Limnol. Sin.* **5** 255–84

Ha K J *et al* 2019 Observations utilizing Korea ocean research stations and their applications for process studies *Bull. Am. Meteorol. Soc.* **100** 2061–75

Haidvogel D B *et al* 2008 Ocean forecasting in terrain-following coordinates formulation and skill assessment of the regional ocean modeling system *J. Comput. Phys.* **227** 3595–624

Han J and Pan H L 2011 Revision of convection and vertical diffusion schemes in the NCEP global forecast system *Weather Forecast.* **26** 520–33

Hazelton A *et al* 2023 2022 real-time Hurricane forecasts from an experimental version of the Hurricane analysis and forecast system (HAFSV0.3S) *Front. Earth Sci.* **11** 1264969

He C, Wang Y, Lei Z and Xu S 1959 A preliminary study of the formation of Yellow Sea cold water mass and its properties *Oceanol. Limnol. Sin.* **2** 1–15 (Chinese with English abstract)

Hersbach H *et al* 2020 The ERA5 global reanalysis *Q. J. R. Meteorol. Soc.* **146** 1999–2049

Hong J S, Moon J H, Kim T, You S H, Byun K Y and Eom H 2022 Role of salinity-induced barrier layer in air-sea interaction during the intensification of a typhoon *Front. Mar. Sci.* **9** 1–16

Hong S-Y and Lim J-O 2006 The WRF single-moment 6-class microphysics scheme (WSM6) *Asia-Pac. J. Atmos. Sci.* **42** 129–51

Hu Y, Yu F, Si G, Sun F, Liu X, Diao X, Chen Z, Nan F and Ren Q 2024 The seasonal evolution of the Yellow Sea cold water mass circulation: roles of fronts, thermoclines, and tidal rectification *Ocean Modelling* **190** 102375

Jiménez P A, Dudhia J, González-Rouco J F, Navarro J, Montávez J P and García-Bustamante E 2012 A revised scheme for the WRF surface layer formulation *Mon. Weather Rev.* **140** 898–918

Knaff J A, Slocum C J, Musgrave K D, Sampson C R and Strahl B R 2016 Using routinely available information to estimate tropical cyclone wind structure *Mon. Weather Rev.* **144** 1233–47

Knaff J A and Zehr R M 2007 Reexamination of tropical cyclone wind-pressure relationships *Weather Forecast.* **22** 71–88

Kwon Y C and Hong S Y 2017 A mass-flux cumulus parameterization scheme across gray-zone resolutions *Mon. Weather Rev.* **145** 583–98

Larson J, Jacob R and Ong E 2005 The model coupling toolkit: a new Fortran90 toolkit for building multiphysics parallel coupled models *Int. J. High Perform. Comput. Appl.* **19** 277–92

Lee S-H and Beardsley R C 1999 Influence of stratification on residual tidal currents in the Yellow Sea *J. Geophys. Res.* **104** 15679–701

Li D, Staneva J, Bidlot J R, Grayek S, Zhu Y and Yin B 2021 Improving regional model skills during typhoon events: a case study for super typhoon lingling over the Northwest Pacific Ocean *Front. Mar. Sci.* **8** 613913

Lie H J, Cho C H, Lee J H and Lee S 2003 Structure and eastward extension of the Changjiang River plume in the East China Sea *J. Geophys. Res.* **108** 1–14

Lin I I, Pun I F and Wu C C 2009 Upper-ocean thermal structure and the western north pacific category 5 typhoons. Part II: dependence on translation speed *Mon. Weather Rev.* **137** 3744–57

Lin I I, Wu C C, Pun I F and Ko D S 2008 Upper-ocean thermal structure and the Western North Pacific category 5 typhoons. Part I: ocean features and the category 5 typhoons' intensification *Mon. Weather Rev.* **136** 3288–306

Lin L, Liu D, Guo X, Luo C and Cheng Y 2020 Tidal effect on water export rate in the Eastern Shelf Seas of China *J. Geophys. Res.* **125** 1–18

Liu B, Guan C, Xie L and Zhao D 2012 An investigation of the effects of wave state and sea spray on an idealized typhoon using an air-sea coupled modeling system *Adv. Atmos. Sci.* **29** 391–406

Liu X, Zhai F, Yan J, Gu Y, Wang Y, Li P and Wu K 2022 Three-dimensional temperature responses to northward-moving typhoons in the shallow stratified Yellow Sea in summer *J. Geophys. Res.* **127** 1–27

Liu Z, Gan J, Hu J, Wu H, Cai Z and Deng Y 2021 Progress on circulation dynamics in the East China Sea and southern Yellow Sea: origination, pathways, and destinations of shelf currents *Prog. Oceanogr.* **193** 102553

Mogensen K S, Magnusson L and Bidlot J-R 2017 Tropical cyclone sensitivity to ocean coupling in the ECMWF coupled model *J. Geophys. Res.* **122** 4392–412

Moon I J and Kwon S J 2012 Impact of upper-ocean thermal structure on the intensity of Korean peninsular landfall typhoons *Prog. Oceanogr.* **105** 61–66

Moon I-J, Shim J-S, Young Lee D, Hak Lee J, Min I-K and Chang Lim K 2010 Typhoon researches using the ieodo ocean research station: part I. Importance and present status of typhoon observation oceanographic division, Korea hydrographic and oceanographic administration (in Korean) *Atmos. Korean Meteorol. Soc.* **20** 247–60

Price J F 1981 Upper ocean response to a hurricane *J. Phys. Oceanogr.* **11** 153–75

Richter D H and Sullivan P P 2013 Sea surface drag and the role of spray *Geophys. Res. Lett.* **40** 656–60

Rogers R *et al* 2013 NOAA'S Hurricane intensity forecasting experiment: a progress report *Bull. Am. Meteorol. Soc.* **94** 859–82

Schade L R and Emanuel K A 1999 The ocean's effect on the intensity of tropical cyclones: results from a simple coupled atmosphere-ocean model *J. Atmos. Sci.* **56** 642–51

Shchepetkin A F and McWilliams J C 2009 Correction and commentary for "Ocean forecasting in terrain-following coordinates: formulation and skill assessment of the regional ocean modeling system by Haidvogel *et al.*, J. Comp. Phys. 227, pp. 3595–3624 *J. Comput. Phys.* **228** 8985–9000

Shin H H and Hong S Y 2013 Analysis of resolved and parameterized vertical transports in convective boundary layers at gray-zone resolutions *J. Atmos. Sci.* **70** 3248–61

Skamarock W C *et al* 2019 A description of the advanced research WRF model version 4 vol 145 (National Center for Atmospheric Research) p 550

Smith R K and Montgomery M T 2016 The efficiency of diabatic heating and tropical cyclone intensification *Q. J. R. Meteorol. Soc.* **142** 2081–6

Sroka S and Emanuel K A 2021 A review of parameterizations for enthalpy and momentum fluxes from sea spray in tropical cyclones *J. Phys. Oceanogr.* **51** 3053–69

Troitskaya Y, Kandaurov A, Ermakova O, Kozlov D, Sergeev D and Zilitinkevich S 2017 Bag-breakup fragmentation as the dominant mechanism of sea-spray production in high winds *Sci. Rep.* **7** 1–4

Troitskaya Y, Kandaurov A, Ermakova O, Kozlov D, Sergeev D and Zilitinkevich S 2018 The "bag breakup" spume droplet generation mechanism at high winds. Part I: spray generation function *J. Phys. Oceanogr.* **48** 2168–88

Wada A, Kanada S and Yamada H 2018 Effect of air-sea environmental conditions and interfacial processes on extremely intense Typhoon Haiyan (2013) *J. Geophys. Res.* **123** 10,379–405

Wada A, Niino H and Nakano H 2009 Roles of vertical turbulent mixing in the ocean response to Typhoon Rex (1998) *J. Oceanogr.* **65** 373–96

Warner J C, Armstrong B, He R and Zambon J B 2010 Development of a coupled ocean-atmosphere-wave-sediment transport (COAWST) modeling system *Ocean Modelling* **35** 230–44

WAVEWATCH III Development Group 2016 User manual and system documentation of WAVEWATCH III version 5.16 *NOAA/NWS/NCEP/MMAB Technical Note 329* pp 1–326

Wei Y, Pei Y and Zhang R H 2015 Seasonal variability of the kuroshio current at the PN section in the East China sea based on *in-situ* observation from 1987 to 2010 *Acta Oceanol. Sin.* **34** 12–21

Xia C, Qiao F, Yang Y, Ma J and Yuan Y 2006 Three-dimensional structure of the summertime circulation in the Yellow Sea from a wave-tide-circulation coupled model *J. Geophys. Res.* **111** 1–19

Xu X, Voermans J J, Ma H, Guan C and Babanin A V 2021 A wind–wave-dependent sea spray volume flux model based on field experiments *J. Mar. Sci. Eng.* **9** 1168

Xu X, Voermans J J, Moon I J, Liu Q, Guan C and Babanin A V 2022 Sea spray impacts on tropical cyclone olwyn using a coupled atmosphere-ocean-wave model *J. Geophys. Res.* **127** 1–13

Yang S, Moon I J, Bae H J, Kim B M, Byun D S and Lee H Y 2022 Intense atmospheric frontogenesis by air–sea coupling processes during the passage of Typhoon Lingling captured at Ieodo ocean research station *Sci. Rep.* **12** 1–14

Yang S, Shin D, Cocke S, Nam C C, Bourassa M A, Cha D-H and Kim B-M 2024 Unveiling the pivotal influence of sea spray heat fluxes on hurricane rapid intensification *Environ. Res. Lett.* **19** 114058

Zhang L, Zhang X, Perrie W, Guan C, Dan B, Sun C, Wu X, Liu K and Li D 2021 Impact of sea spray and sea surface roughness on the upper ocean response to super Typhoon Haitang (2005) *J. Phys. Oceanogr.* **51** 1929–45